Incoherent scattering of 279, 322, 662 and 1115 keV gamma rays in Cu, Sn and Pb

1980 J. Phys. B: At. Mol. Phys. 13 273

(http://iopscience.iop.org/0022-3700/13/2/015)

J. Phys. B: Atom. Molec. Phys. **13** (1980) 273–282. Printed in Great Britain

Incoherent scattering of 279, 322, 662 and 1115 keV gamma rays in Cu, Sn and Pb

Shivaramu, S Gopal and B Sanjeevaiah

Department of Physics, University of Mysore, Manasagangotri, Mysore 570 006, India

Received 6 June 1979, in final form 20 July 1979

Abstract. The differential incoherent scattering cross sections of 279 and 322 keV photons in copper, tin and lead were experimentally determined at different angles ranging from 10–120° by the method of Shivaramu, Gopal and Sanjeevaiah. The cross sections of 662 and 1115 keV photons were also experimentally determined in copper, tin and lead using a cone geometry between 3 and 8°. The incoherent scattering functions derived from the experimental results agree fairly well with the values calculated by Cromer on the basis of SCF Hartree–Fock wavefunctions.

1. Introduction

Incoherent scattering is one of the major processes by which gamma rays interact with matter in the energy range from 0·1 to 5 MeV. The knowledge of the incoherent scattering function is important to understand the small-angle inelastic scattering of charged particles and the production of bremsstrahlung and of positron–electron pairs in the field of electrons (Grodstein 1957). The data on differential and integral incoherent scattering cross sections are very useful in calculating radiation attenuation, transport and energy deposition in medical physics, reactor shielding, industrial radiography and in a variety of other areas in addition to x-ray crystallography (Hubbell *et al* 1975).

The values of the incoherent scattering function $S(h\nu, \theta, Z)$ given in Hubbell *et al* (1975) reveal the paucity of the whole atomic differential data. Owing to the theoretical developments by Cromer and Mann (1967, 1968) and Cromer (1969), improved theoretical values of incoherent scattering functions are now available based on SCF Hartree–Fock wavefunctions. As pointed out by Ramanathan *et al* (1979), calculated incoherent scattering functions have not been put to a completely rigorous experimental test. Differential incoherent scattering cross sections have been measured at 662 keV in iron at 20 to 90° (Singh *et al* 1963), in lead at 20 to 160° (Quivy 1966), in lead at 62, 85 and 135° (Schumacher 1971), at 662 and 1115 keV in copper, tin, mercury, tungsten and lead at 2 to 165° (Sinha *et al* 1976) and at 1170 and 1330 keV energy in lead at 4 to 8° (Kane *et al* 1978). All these studies have been made at photon energies of 662 keV or greater.

Therefore it was considered worthwhile to determine differential incoherent scattering cross sections experimentally at different angles ranging from 10 to 120° using 279 and 322 keV gamma rays following the method of Shivaramu *et al* (1977, 1978). The cross sections below 10° were not determined at the above energies because the

0022-3700/80/020273+10$01.00

coherent contribution in the scattered beam becomes dominant. Incoherent scattering cross sections for the energies 662 and 1115 keV were also measured using cone geometry at angles between 3 and 8°. In this geometry an extrapolation method described in § 3 was followed to minimise multiple scattering, self absorption and sample-dependent background in the scatterer. The measured incoherent scattering cross sections and the incoherent scattering functions derived from the measured cross sections are compared with the theoretical values of Cromer (1969).

2. Experimental methods

2.1. Cylindrical geometry for the measurement of incoherent scattering cross sections above 10° at 279 and 332 keV photon energies

The experimental arrangement used in the present investigation is the same as that described earlier (Shivaramu *et al* 1977). The photons of energy 279 and 322 keV emitted from the 500 mCi ^{203}Hg and ^{51}Cr sources (in the form of radiographic capsules obtained from the Bhabha Atomic Research Centre, Bombay) were collimated and made to fall on the cylindrical scatterers of different radii. The distance between the source and scatterer was 36 cm and that between the scatterer and detector was 100 cm. The copper cylinders were 0·40–0·85 cm in diameter, the tin cylinders 0·45–0·85 cm in diameter and the lead cylinders 0·2–0·7 cm in diameter. The photopeaks of the collimated scattered radiation at different angles ranging from 10 to 120° were recorded with a gamma ray spectrometer consisting of a NaI(Tl) crystal 2·54 cm long and 2·54 cm diameter coupled to a 1024 Channel analyser.

2.2. Cone geometry for the measurement of incoherent scattering cross sections below 10° at 662 and 1115 keV photon energies

The cylindrical geometry cannot be adopted to measure the cross sections below 10° due to the dead space caused by the straight photon beam from the source. Therefore at angles less than 10° a shadow cone type experimental arrangement was used and is shown in figure 1. The isotopes ^{137}Cs and ^{65}Zn of strengths 450 and 100 mCi in the form of radiographic capsules (obtained from the Radio Chemical Centre, Amersham,

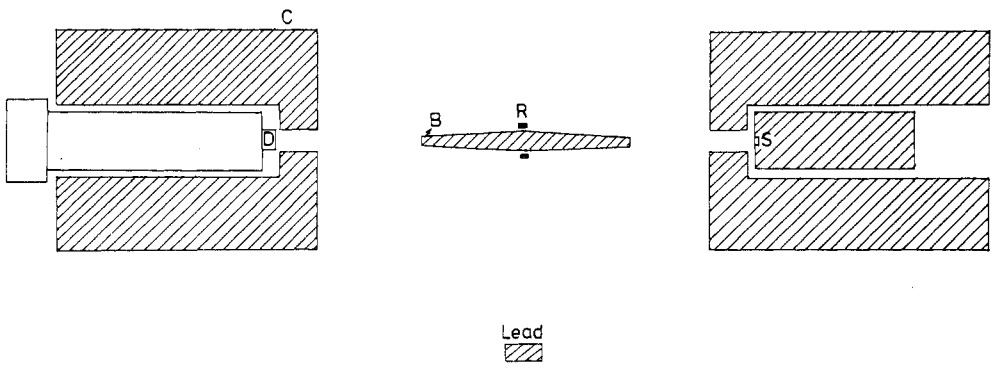

Figure 1. Schematic diagram (not to scale) of the experimental system: S, source; R, Ring scatterer; D, NaI(Tl) crystal detector; B, Beam stopper; C, lead collimator.

England and Bhabha Atomic Research Centre, Bombay respectively) were used. The source and the detector were provided with adequate lead shielding for reducing the background to a low level. The direct gamma beam is prevented from reaching the NaI(Tl) detector. The outer part of the beam is absorbed by the lead collimator C(1·35 cm inner diameter and 30 cm long) and the inner part of the beam by the lead absorber (3 cm diameter at the centre and 2 cm at the end and 20 cm long). Ideally the only radiation which can reach the detector is that scattered by the ring target. The source to detector distance was 250 cm and the distance between the scatterer and the detector was varied to change the scattering angle.

The ring scatterers of copper, tin and lead had axial thickness between 0·2 to 1 cm. The angular width of all scatterers was 1 cm. The entire assembly consisting of the source, the lead absorber having a double cone shape and the detector was optically aligned with a cathetometer. The constancy of the photopeak counting rate at different positions of an auxiliary source at the same radial distance from the axis of the double cone lead absorber provided a check of the correct alignment. The photopeaks of the scattered radiation at different angles ranging from 3 to 8° were recorded with the same gamma ray spectrometer described earlier.

2.3. Measurements

The photopeaks of the gamma photons scattered from cylindrical scatterers of different elements having different radii were recorded at each angle between 10 and 120° in the cylindrical geometry. A typical resultant photopeak of the scattered spectrum after the background was subtracted is shown in figure 2(a) obtained using 279 keV gamma rays and a tin cylindrical scatterer of radius 0·86 cm at $\theta = 20°$.

Similarly the photopeaks of the gamma photons scattered from ring scatterers of different elements having different axial thickness were recorded at each angle between 3 and 8° in the cone geometry. Figure 2(b) shows the resulting photopeak of the scattered spectrum after the background was subtracted at 662 keV energy with a tin scatterer of 0·48 cm axial thickness and 7 cm mean diameter corresponding to a scattering angle of 6°. In the case of ring scatterers there is always a heavy background due to the large solid angle subtended by the detector at the scatterer. When the background is subtracted from the spectrum obtained with scatterer in position the Compton edge in this case (figure 2(b)) is not so pronounced as in the case of cylindrical scatterers (figure 2(a)). Weak auxiliary sources were kept at the place of the scatterer and the spectra were recorded.

2.4. Determination of cross sections

In the auxiliary source method the differential cross section for the scattering of gamma rays by a target atom is given by the formula

$$\frac{d\sigma}{d\Omega} = \left(\frac{n_c}{N}\right)\left(\frac{1}{n_b}\right)\left(\frac{B}{A}\right) r^2 \frac{\epsilon_b}{\epsilon_c} \tag{1}$$

where n_c is the net photopeak counting rate with a main source of strength A, n_b is the corresponding net counting rate measured with the weak auxiliary source of strength B at the scatterer position, r is the source to scatterer distance and N is the number of scattering atoms, ϵ_b and ϵ_c are the corresponding photopeak efficiencies for incident and scattered energies.

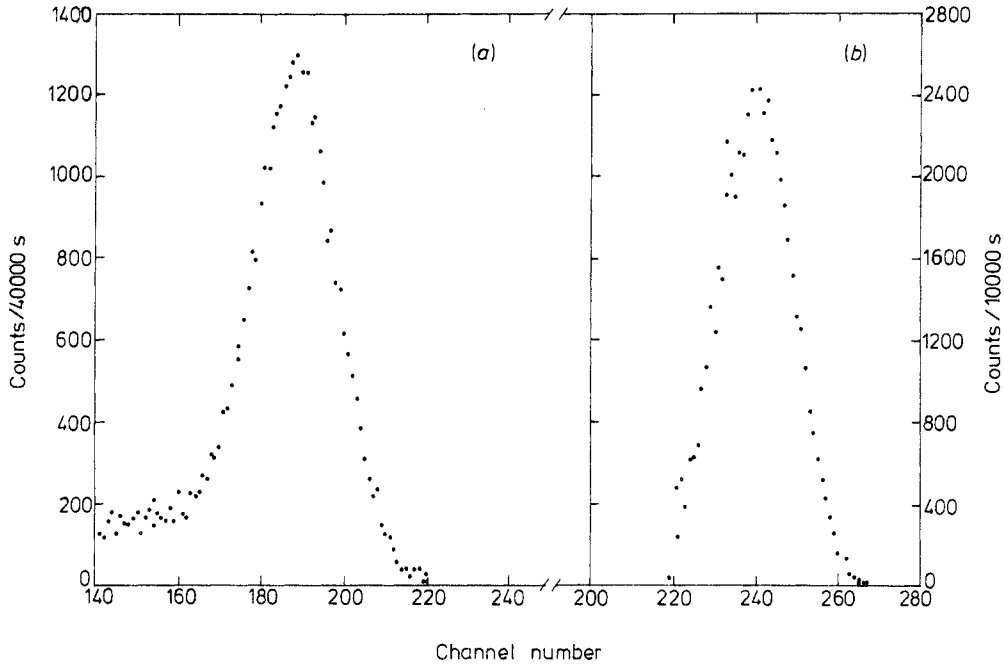

Figure 2. Resultant photopeaks of the scattered spectra after the background is subtracted for $Z = 50$; (a) using 279 keV gamma rays and a tin cylindrical scatterer of radius 0·86 cm at $\theta = 20°$; (b) using 662 keV gamma rays with a tin scatterer of 0·48 cm axial thickness, at $\theta = 6°$.

2.5. Corrections and errors

Some of the photons contributing to the background will be absorbed when the sample is introduced. The net effect is the reduction in the observed background. The attenuation of the background in the presence of the sample depends on the thickness of the sample seen by the background radiation. A graph of $\lg(n_c/N)$ versus the thickness of the scatterer is shown in figure 3(a). The error on the $\lg(n_c/N)$ values are less than one per cent in all cases and they are within the dimensions of the points marked. It may be seen that this plot is a straight line within the limits of errors and hence the sample dependent background is automatically corrected when $\lg(n_c/N)$ is extrapolated to zero thickness.

In the case of small angle scattering the cross section varies rapidly with the scattering angle. There is always a spread in the angular acceptance of the detector. This arises because of the finite extension of the source, scatterer and detector. The measured cross section was corrected for this effect using the relation given by Nath and Ghose (1964). Uncertainties in the correction can give rise to an associated error up to two per cent. In the case of cylindrical geometry the spread in the scattering angle was within ±2°. The correction for this is found to be negligible.

Since we do not use the absolute strength of the source, its self absorption has no effect on our measurements. The ratios (n_c/n_b) were obtained with statistical uncertainties of less than one per cent except for lead at larger angles. The number of scattering atoms (N) in the ring scatterer is proportional to (M/A) where M is the mass

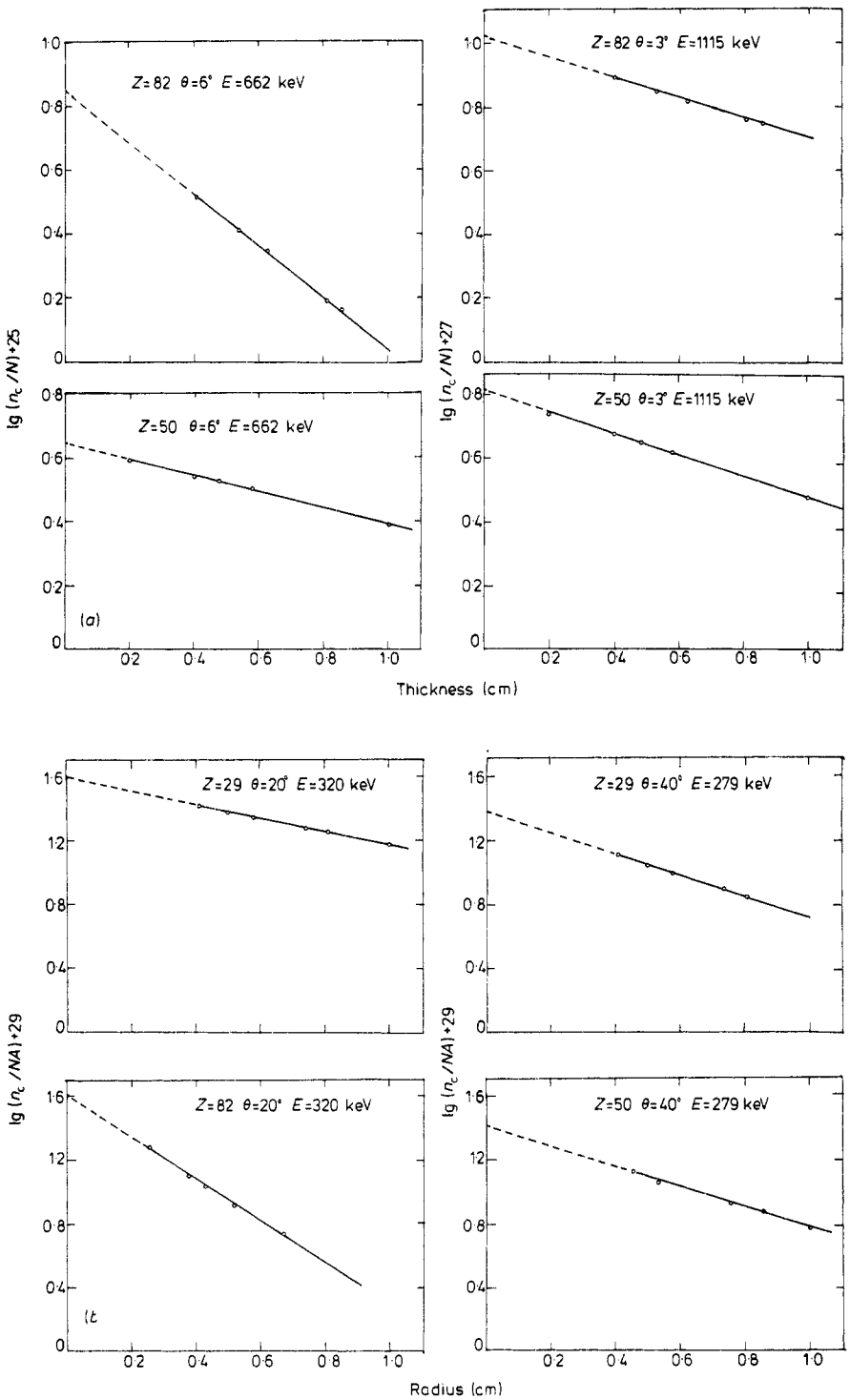

Figure 3. (a) $\lg(n_c/N)$ as a function of thickness of the ring scatterer. (b) $\lg(n_c/NA)$ as a function of radius of the cylindrical scatterer.

of the scatterer and A is the atomic weight of the scatterer. The mass, M, of the scatterer was determined to an accuracy better than 0·1%. The purity of all the scatterers used was found to be 99·9% by the chemical analysis. The thickness of the ring scatterers was determined by weighing. This was checked by micrometer measurements to ensure that the material density was normal. In the case of cylindrical geometry the number of atoms (N) present in the scatterer can be determined accurately by knowing the length of the scatterer exposed to the incident beam. The error on N was negligible. The ratio (B/A) was found by comparing the areas of the photopeaks of the spectra recorded directly with the two sources in the same geometry, this error was less than 2 per cent. The relative photopeak efficiencies of the detector for various gamma ray energies were computed theoretically from the work of Gardner (1976). The values of the photofractions computed theoretically were compared with the experimental values of the photofractions obtained from the scattered spectra. There is agreement within an average relative standard deviation of three per cent between computed and experimental values. The product of computed intrinsic efficiency and the photofraction gives the photopeak efficiency for a particular gamma ray energy. The uncertainties in correcting for the coherent contribution at small scattering angles would introduce an error of nearly two per cent. The combined error on the measured scattering cross section varied between 5 and 8 per cent.

3. Results and discussion

The values of n_c were recorded for scatterers of different radii of the cylindrical scatterer and axial thickness of the ring scatterer and (n_c/N) values were substituted in the equation (1) to calculate the differential scattering cross sections. The values of the differential scattering cross sections so obtained were found to depend on the axial thickness of the ring scatterer and the radius of the cylindrical scatterer respectively showing that multiple scattering and self absorption depend on these parameters. The values of $\lg(n_c/N)$ were plotted as functions of different axial thickness of the ring scatterer and radii of the cylindrical scatterer and are illustrated in figures 3(a) and (b). The decrease of $\lg(n_c/N)$ values as the axial thickness of the ring scatterer and radius of the cylindrical scatterer increase can be attributed to self absorption and multiple scattering in the scatterer. Self absorption in the scatterer is due to the absorption of the incident and scattered photons inside the scatterer. The probability of the absorption of primary photons and scattered photons is proportional to the axial thickness of the ring scatterer and to the radius of the cylindrical scatterer respectively; Ramanathan *et al* (1979) give a more detailed discussion of this point. The multiple scattering is largely proportional to the thickness of the ring scatterer and to the radius of the cylindrical scatterer. A square root dependence of multiple scattering on the thickness of the scatterer was suggested by Lichtenberg and Przybylski (1972). Tanner and Epstein (1974) have also noticed a square root dependence of multiple scattering on the thickness of the scatterer. This is one of the important problems which is often neglected in incoherent scattering cross section measurements. If $\lg(n_c/N)$ is extrapolated to zero thickness of the ring scatterer and to the zero radius of the cylindrical scatterer the self absorption and multiple scattering will be minimised to a greater extent. The extrapolated values of $\lg(n_c/N)$ to the zero thickness of the ring scatterer and to the zero radius of the cylindrical scatterer were used to calculate the differential scattering cross sections.

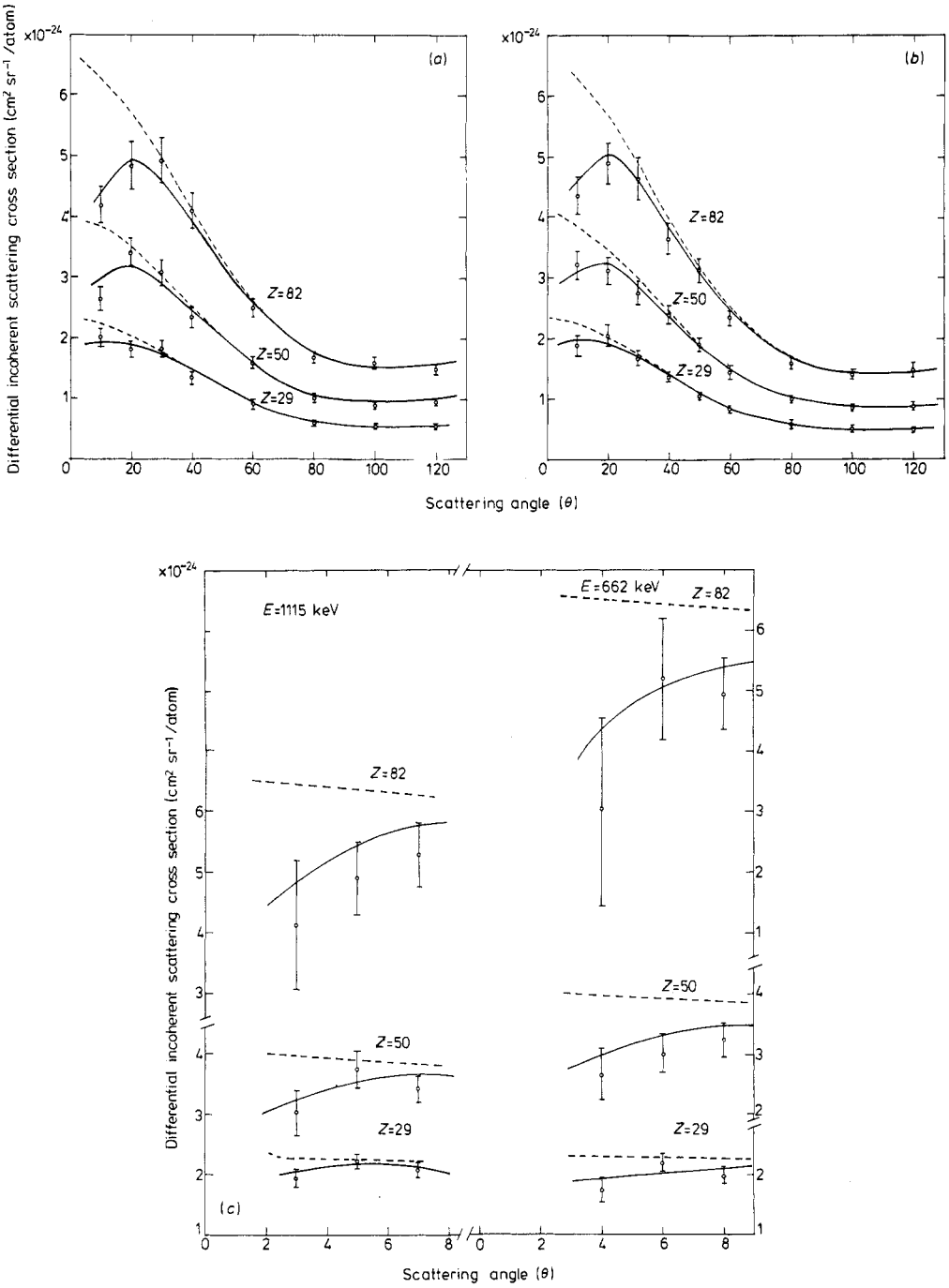

Figure 4. Differential incoherent scattering cross sections as a function of scattering angle. The curve is traced from the theory of Cromer based on SCF Hartree–Fock wavefunctions. The broken curve is calculated from the Klein–Nishina formula. The points marked represent experimental results. (a) $E = 279$ keV, (b) 320 keV, (c) 662 and 1115 keV.

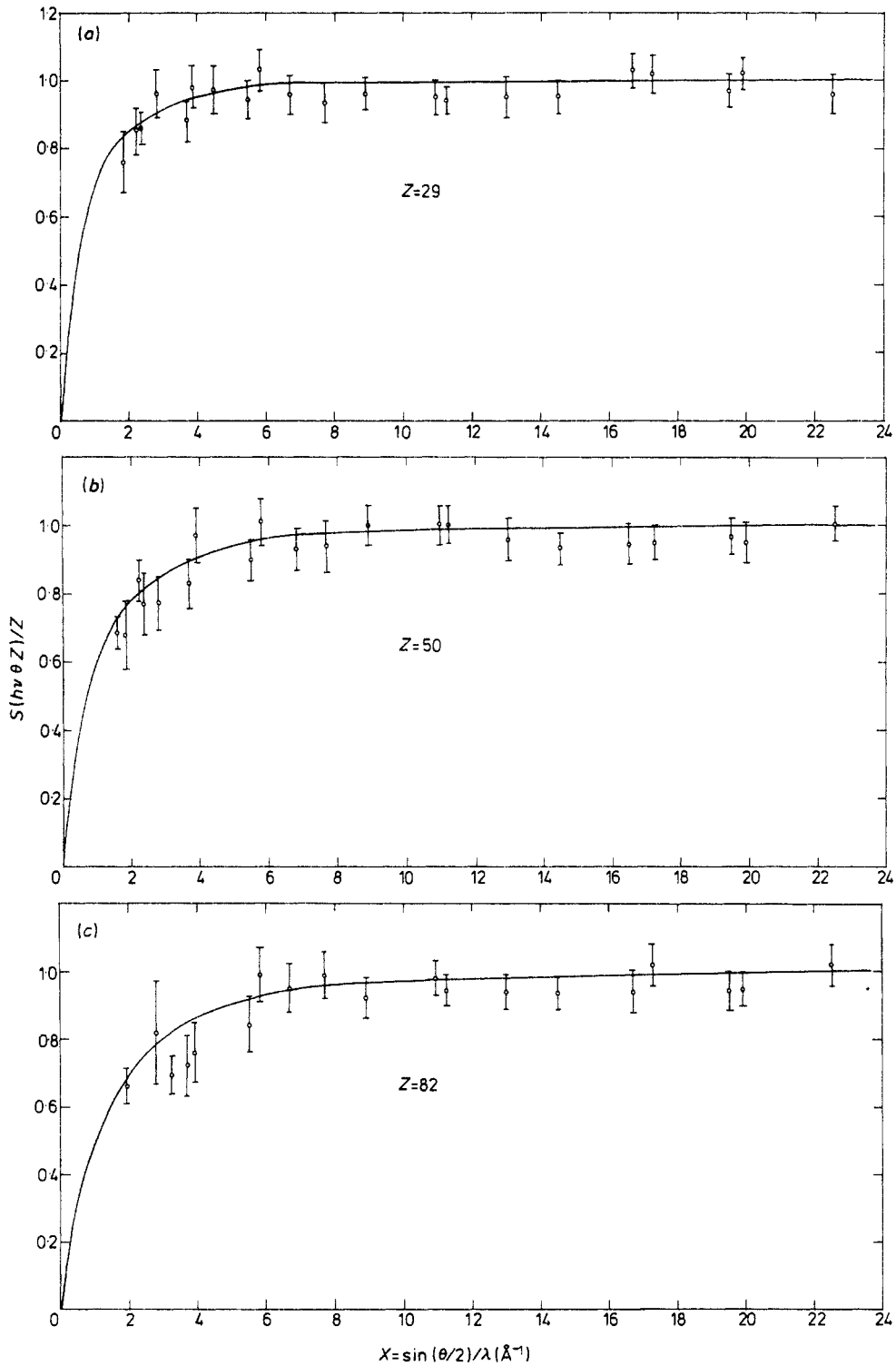

Figure 5. Incoherent scattering function $S(h\nu, \theta, Z)$ as a function of $X = \sin(\frac{1}{2}\theta)/\lambda(\text{Å})$. The curve is based on Cromer's non-relativistic SCF Hartree–Fock calculations. The points marked represent experimental results. (a) $Z = 29$, (b) $Z = 50$, (c) $Z = 82$.

For scattering angles of 40° or more the coherent scattering photons were clearly separated from the incoherently scattered photons. On the other hand for $\theta < 40°$ the incoherently and coherently scattered photons were not resolved. In the case of cone geometry measurements i.e. at angles below 10° we have measured the total differential scattering cross section. This can be written as:

$$\left(\frac{d\sigma}{d\Omega}\right)_{tot} = \left(\frac{d\sigma}{d\Omega}\right)_{incoh} + \left(\frac{d\sigma}{d\Omega}\right)_{coh}$$

where $(d\sigma/d\Omega)_{incoh}$ is the differential incoherent scattering cross section, $(d\sigma/d\Omega)_{coh}$ is the differential coherent scattering cross section and we have neglected the small difference in photopeak efficiencies of coherent and incoherent scattered photons arising from the fact that the incoherent component differs slightly in energy from the coherent component. The theoretically calculated coherent scattering cross section was subtracted to obtain the incoherent scattering cross section. In the case of scattering angles at θ equals 10, 20 and 30° the change in the energy of the incoherent photons is more than two per cent compared with primary photons and so, it is no longer justified to neglect the effects of energy loss of the incoherent component. We corrected for the small coherent component in terms of the measured photopeak count at a scattering angle, θ of 40° and the known theoretical differential coherent scattering cross sections at low angles. Theoretical coherent scattering cross sections were calculated using relativistic $F(x, Z)$ values tabulated by Hubbell and Øverbø (1979) based on SCF Hartree–Fock wavefunctions.

The experimental values of the incoherent scattering cross sections and Klein–Nishina (1929) cross sections together with the cross sections evaluated on the basis of Cromer's SCF Hartree–Fock wavefunctions tabulated by Hubbell *et al* (1975) are displayed in figures 4(a), (b) and (c) for different elements and energies at different momentum transfers. The data represented in these figures are in general agreement with the incoherent function formalism. The angular region investigated definitely reveals the lowering of the forward scattering cross sections compared with the Klein–Nishina (1929) values that may be attributed to the effect of electron binding.

From the measured incoherent scattering cross sections, the $S(h\nu, \theta, Z)$ values were computed using the relation

$$\left(\frac{d\sigma}{d\Omega}\right)_{incoh} = \left(\frac{d\sigma}{d\Omega}\right)_{KN} S(h\nu, \theta, Z)$$

where $S(h\nu, \theta, Z)$ is the incoherent scattering function and $(d\sigma/d\Omega)_{KN}$ is the theoretical Klein–Nishina differential scattering cross section. Experimental values of $S(h\nu, \theta, Z)$ for copper, tin and lead are shown in figures 5(a), (b) and (c) for different values of momentum transfers. The full curves in figures 5(a), (b) and (c) represent the values of Hubbell *et al* (1975) obtained on the basis of the non-relativistic Hartree–Fock theory. Good agreement is seen between the experimental and theoretical values.

Acknowledgment

One of the authors (SR) thanks the Council of Scientific and Industrial Research, India, for awarding him a Senior Research Fellowship.

References

Cromer D T 1969 *J. Chem. Phys.* **50** 4857–59
Cromer D T and Mann J B 1967 *J. Chem. Phys.* **47** 1892–3
—— 1968 *Acta Cryst.* A **24** 321–4
Gardner R P 1976 *Nucl. Instrum. Meth.* **138** 287–91
Grodstein G W 1957 *NBS Circular* No 583 (Washington DC: US Govt. Printing Office)
Hubbell J H, Veigele W J, Briggs E A, Brown R T, Cromer D T and Howerton R J 1975 *J. Phys. Chem. Ref. Data* **4** 471–538
Hubbell J H and Øverbø I 1979 *J. Phys. Chem. Ref. Data* **8** 69–105
Kane P P, Basavaraju G, Mahajani J and Priya Darshini A K 1978 *Nucl. Instrum. Meth.* **155** 467–74
Klein O and Nishina Z 1929 *Z. Phys.* **52** 853–68
Lichtenberg W and Przybylski A 1972 *Nucl. Instrum. Meth.* **98** 99
Nath A and Ghose A M 1964 *Nucl. Phys.* **57** 547–64
Quivy R 1966 *Nucl. Phys.* **76** 362–6
Ramanathan N, Kennett T J and Prestwich W V 1979 *Can. J. Phys.* **57** 343–52
Schumacher M 1971 *Z. Phys.* **242** 444–57
Shivaramu, Gopal S and Sanjeevaiah B 1977 *Nucl. Instrum. Meth.* **140** 529–32
—— 1978 *J. Phys. B: Atom. Molec. Phys.* **11** 1123–27
Singh M, Anand S and Sood B S 1963 *Ind. J. Pure Appl. Phys.* **1** 305–7
Sinha B, Roy S C and Chaudhuri N 1976 *J. Phys. B: Atom. Molec. Phys.* **9** 3185–91
Tanner A C and Epstein I R 1974 *J. Chem. Phys.* **61** 4251–57